# Dynamic scaling of stochastic thermodynamic observables for chemical reactions at and away from equilibrium

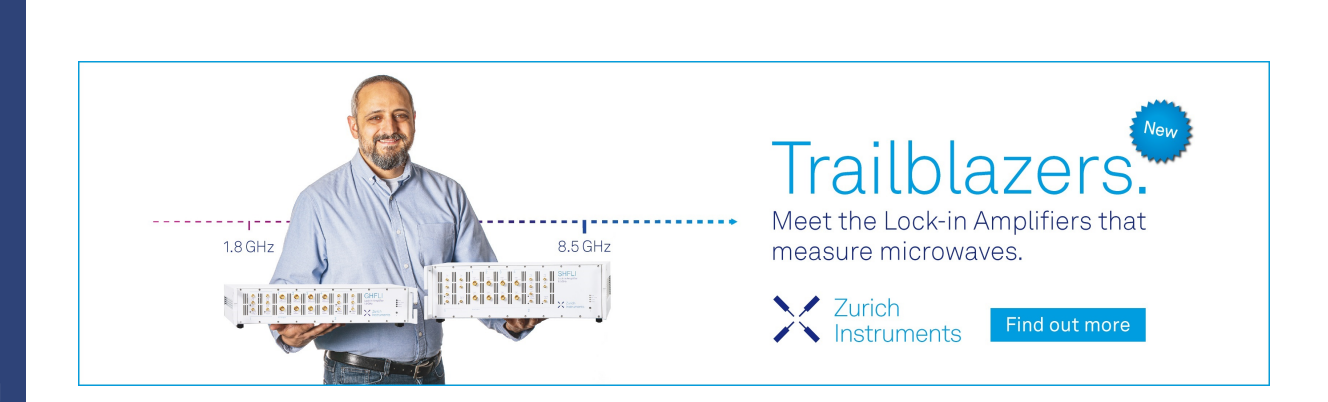
Cite as: J. Chem. Phys. **157**, 194105 (2022); https://doi.org/10.1063/5.0106714 Submitted: 29 June 2022 • Accepted: 25 October 2022 • Published Online: 16 November 2022













## Dynamic scaling of stochastic thermodynamic observables for chemical reactions at and away from equilibrium

Cite as: J. Chem. Phys. 157, 194105 (2022); doi: 10.1063/5.0106714

Submitted: 29 June 2022 • Accepted: 25 October 2022 •

**Published Online: 16 November 2022** 











Shrabani Mondal, 1,2 D Jonah S. Greenberg, 1,3 D and Jason R. Green 1,4,a)



#### **AFFILIATIONS**

- Department of Chemistry, University of Massachusetts Boston, Boston, Massachusetts 02125, USA
- <sup>2</sup>Department of Chemistry, Physical Chemistry Section, Jadavpur University, Kolkata 700032, India
- <sup>3</sup>Department of Chemistry, Northwestern University, Evanston, Illinois 60208, USA
- Department of Physics, University of Massachusetts Boston, Boston, Massachusetts 02125, USA

#### **ABSTRACT**

Physical kinetic roughening processes are well-known to exhibit universal scaling of observables that fluctuate in space and time. Are there analogous dynamic scaling laws that are unique to the chemical reaction mechanisms available synthetically and occurring naturally? Here, we formulate an approach to the dynamic scaling of stochastic fluctuations in thermodynamic observables at and away from equilibrium. Both analytical expressions and numerical simulations confirm our dynamic scaling ansatz with associated scaling exponents, function, and law. A survey of common chemical mechanisms reveals classes that organize according to the molecularity of the reactions involved, the nature of the reaction vessel and external reservoirs, (non)equilibrium conditions, and the extent of autocatalysis in the reaction network. Varying experimental parameters, such as temperature, can cause coupled reactions capable of chemical feedback to transition between these classes. While path observables, such as the dynamical activity, have scaling exponents that are time-independent, the variance in the entropy production and flow can have time-dependent scaling exponents and self-averaging properties as a result of temporal correlations that emerge during thermodynamically irreversible processes. Altogether, these results establish dynamic universality classes in the nonequilibrium fluctuations of thermodynamic observables for well-mixed chemical reactions.

Published under an exclusive license by AIP Publishing. https://doi.org/10.1063/5.0106714

#### I. INTRODUCTION

Chemical reaction mechanisms have the functionality and the diversity to create materials, synthesize medications, and sustain life. However, these kinetic mechanisms can be difficult to classify because of this diversity and their nonequilibrium nature. By contrast, it is well known in statistical physics that seemingly unrelated physical phenomena, from sandpiles to earthquakes, can share universal laws when we change the time and length scale of our observation.<sup>1,2</sup> Moreover, simulations of and experiments<sup>3-6</sup> on growing interfaces have shown that concepts of scaling and universality can apply beyond equilibrium critical phenomena to systems driven out of equilibrium. Despite this progress for physical phenomena, it is unclear whether there are complementary dynamic scaling laws for chemical reactions.

Universal scaling behavior has been found in biochemical networks,8 the stochastic exponential growth and division of bacterial cells, 9,10 the growth of human cancers,11 and dissipative self-assembly. 12 Formal analogies have expanded the scope of kinetic roughening theory 13,14 even further by treating the fluctuations of mathematical functions as surrogates for the physical interface.1 Examples include biological systems, such as DNA, 15 complex networks, 16 crude oil prices, 17 heartbeat signals, 18 strongly interacting gases, 19 and material fracture. 20 Applying this idea to the Lyapunov exponents of dynamical systems, for example, has revealed that the leading Lyapunov vector of extended dissipative dynamical systems<sup>21–24</sup> falls within the Kardar, Parisi, and Zhang universality class.<sup>25</sup> Hamiltonian dynamical systems show anomalous non-KPZ behavior; long-range correlations can cause the fluctuations in finite-time Lyapunov exponents in these systems to self-average

a) Author to whom correspondence should be addressed: jason.green@umb.edu

weakly<sup>26,27</sup> and even diverge.<sup>28</sup> These results highlight not only the breadth of kinetic roughening theory but also how dynamical mechanisms can influence universal behavior. Given the diversity of chemical transformations, they also motivate a deeper look at the dynamic scaling and potential universality classes of chemical reactions.

Chemical reactions are dynamic phenomena involving transformations of energy, which makes the fluctuating observables of stochastic thermodynamics good candidates for an analogy with surface roughening. In the framework of stochastic thermodynamics, <sup>29–31</sup> quantities, such as heat, work, and entropy, can be treated at the level of individual, fluctuating trajectories. Nonequilibrium fluctuations are known to obey strong relations, including fluctuation theorems and thermodynamic uncertainty relations,<sup>32-34</sup> some of which can be cast as thermodynamic speed limits.<sup>35–39</sup> Here, we show the fluctuations of thermodynamic observables also satisfy a dynamical scaling hypothesis in well-mixed chemical reaction systems. We do this by analyzing the nonequilibrium fluctuations in stochastic thermodynamic observables of a broad set of elementary and coupled chemical reactions at and away from equilibrium. Numerical and analytical agreement with our scaling hypotheses suggest the division of fluctuations in dynamical observables into distinct classes. The corresponding scaling exponents do not depend on the molecular nature of the chemical species. In some cases, the exponents are also independent of the reactions conditions, such as temperature, or whether the reaction vessel is open or closed to the flux of matter. Our approach here enables us to divide chemical kinetic processes into classes according to the values of these characteristic scaling exponents.

#### **II. MODEL AND METHODS**

#### A. Well-mixed chemical reaction systems

To model systems of chemical reactions, we adopt a standard framework at the mesoscopic level: we consider well-mixed chemical populations of finite number in a reaction vessel with volume V. Each system we consider consists of n chemical species  $\mathbf{X} := (X_1, X_2, \ldots, X_n)^{\mathsf{T}}$ , with  $X_k$  representing the number of molecules of the kth species at a time t and  $\mathsf{T}$  denoting the transpose. A total of m reactions are possible, each reaction having a stoichiometric or state-change vector  $\mathbf{v}_j \in \mathbb{R}^n$  whose ith element is the change in the number of  $X_i$  molecules caused by the jth reaction. The evolution of the entire mixture is governed by the chemical master equation, i0 which for the time evolution of the probability distribution, i1 which for the time evolution of the probability distribution, i2 which for the time evolution of the probability distribution, i3 which for the time evolution of the probability distribution, i4 which for the time evolution of the probability distribution, i5 which for the time evolution of the probability distribution, i6 which for the time evolution of the probability distribution, i6 which for the time evolution of the probability distribution, i6 which for the time evolution of the probability distribution, i6 which for the time evolution of the probability distribution, i6 which for the time evolution of the probability distribution, i6 which for the time evolution of the probability distribution, i8 which for the time i8 which for the i8 which for the i8 which for the i9 which i9 wh

$$\frac{dP(\mathbf{X},t)}{dt} = \sum_{j=1}^{m} a_j (\mathbf{X} - \mathbf{v}_j, t) P(\mathbf{X} - \mathbf{v}_j, t) - \sum_{j=1}^{m} a_j (\mathbf{X}, t) P(\mathbf{X}, t). \quad (1)$$

The propensity function,  $a_j(\mathbf{X},t)$ , determines the probability,  $a_j(\mathbf{X},t)dt$ , that the jth reaction occurs in an infinitesimal time interval [t,t+dt). The propensity also depends on b, which is the molecularity for elementary reactions. For example, unimolecular reactions,  $A \to \emptyset$ , have a propensity  $c_j X_A(t)$  with stochastic rate constant  $c_j \propto 1$ ; bimolecular reactions,  $A + B \to \emptyset$ , have a propensity  $c_j X_A(t) X_B(t)$  with  $c_j \propto 1/V$ . The total propensity,  $a(\mathbf{X},t) = \sum_{j=1}^{m} a_j(\mathbf{X},t)$ , is the sum of the propensities for all

m-reactions. The rate constants  $k_j$  of each reaction are related to the stochastic rate constant  $c_j$  through combinations of the volume and Avogadro's number  $N_A$  that depend on the reaction molecularity. For example, for a second-order reaction, the relation is  $c_j = k_j/N_A V$ . Here, we fix V so that  $c_j$  does not depend on the number of molecules.

The chemical master equation can be solved numerically with the finite-state projection method, 42,43 thresholding, 44 and the stochastic simulation algorithm.<sup>45</sup> To extract scaling laws and scaling exponents, we use stochastic simulations of the chemical kinetics, kinetic Monte Carlo using the Doob-Gillespie algorithm. 46-48 This algorithm generates stochastic realizations (trajectories) of the chemical kinetics. An ensemble of these trajectories is a statistical sample of the distribution that is the solution to the chemical master equation. 49,50 Each realization represents the composition (number of molecules of each chemical species) of a mixture of *N* molecules in a volume *V* evolving over time. That is, the mixture advances through a time-ordered sequence of chemical compositions  $\hat{\mathbf{X}}(t) = {\mathbf{X}(t_n), \dots, \mathbf{X}(t_0)}$  as a result of chemical reaction events with exponentially-distributed waiting times.<sup>41</sup> Our simulations of these stochastic trajectories require a chemical mechanism (the elementary or composite reaction and their associated rate constants) and experimental conditions, such as volume, temperature, and initial number of molecules. In the results that follow, we simulate a wide range of reactions, varying rate parameters, temperature, and initial number of reactants for each reactive system of interest.

#### B. Stochastic thermodynamics and kinetics

Fluctuations in several thermodynamic observables fit within the scaling theory we present here. For example, the number of configuration changes in the reaction mixture over a given time interval is a common measure of the lability of the dynamics through configuration space (of chemical compositions).<sup>51</sup> This "dynamical activity,"  $K[\hat{\mathbf{X}}(t)]$ , for each stochastic trajectory  $\hat{\mathbf{X}}(t)$  is the number of reactions occurring in a mixture of N molecules over an observation time  $t = t_f - t_0$ . In practice, we add one to the reaction count,  $K[\hat{\mathbf{X}}(t)]$ , at each time a reaction occurs during the observation time. We define this path functional, and others, more simply as  $K(x, N, t) := K[\hat{\mathbf{X}}_x(t)]$  to emphasize the label or "trajectory index" x that identifies a particular stochastic realization of the reaction process. For other model systems, this counting observable has revealed dynamical phase transitions.<sup>52</sup> Even for the well-mixed reaction vessels we consider here, its distribution over trajectory ensembles is not necessarily Poissonian.

Complementing the work of others on the stochastic thermodynamics of chemical reaction networks (e.g., Refs. 53–57), we analyze the entropy flow, which is directly related to the heat dissipated to or absorbed from surroundings for systems that are local detailed balanced. <sup>58,59</sup> For a single stochastic realization of the reaction process, the action functional, <sup>60</sup>

$$Q_s(x, N, t) = \sum_{i=0}^{K(t)-1} \ln \frac{a_i(\mathbf{X} \to \mathbf{X} + \mathbf{v}_i, t_i)}{a_i(\mathbf{X} + \mathbf{v}_i \to \mathbf{X}, t_i)},$$
 (2)

is often interpreted as the entropy exchanged between the system and the environment.  $^{54,61}$  Here,  $a_i$  is the propensity of the reaction

that occurs at time  $t_i$  along a particular stochastic trajectory,  $\hat{\mathbf{X}}_x$ , when the reaction mixture has composition  $\mathbf{X}$ . This "entropy flow,"  $Q_s(x,N,t)=-\Delta s_e$ , is accumulated over the K reactions that occur up to a time t. So, for each realization labeled by x, this observable depends on t and the number of molecules, N (through the propensities of the reactions along the stochastic trajectory). The subscript on  $Q_s$  indicates the connection to the entropy flow. This connection follows from the decomposition of the entropy change for the system along the path,

$$\Delta s = \Delta s_i + \Delta s_e = -\ln \frac{P(\mathbf{X}, t)}{P(\mathbf{X}, t_0)},\tag{3}$$

into contributions from the entropy flow and the entropy production internal to the system  $\Delta s_i$ . This partitioning also applies to ensemble averages in stochastic thermodynamics where, for local detailed balanced systems, the entropy production,  $\Delta S_i \geq 0$ , is nonnegative and vanishes at thermodynamic equilibrium, a statement of the second law of thermodynamics.<sup>31</sup>

The entropy production and flow decompose into observables used in information theory and dynamical systems using the branching observables for a forward path

$$Q_{+}(x, N, t) = \sum_{i=0}^{K(t)-1} \ln \frac{a_{i}(\mathbf{X} \to \mathbf{X} + \mathbf{v}_{i}, t_{i})}{a(\mathbf{X}, t_{i})}$$
(4)

and its conjugate reverse

$$Q_{-}(x,N,t) = \sum_{i=0}^{K(t)-1} \ln \frac{a_i(\mathbf{X} + \mathbf{v}_i \to \mathbf{X}, t_i)}{a(\mathbf{X} + \mathbf{v}_i, t_i)} + \ln \frac{a(\mathbf{X},t)}{a(\mathbf{X}, t_0)}.$$
 (5)

Here, the subscripts + and – indicate the forward and reverse paths, respectively. At steady-state, the trajectory-average of  $Q_+$  is related to the dynamical entropy per unit time  $h_{KS}(N) = -\lim_{t\to\infty} \langle Q_+ \rangle/t$  in information theory (the analog of the Kolmogorov–Sinai entropy rate in dynamical systems theory). These observables measure the degree of branching along a particular forward (or reverse) stochastic path. Together,  $-\Delta s_e = Q_s = Q_+ - Q_-$ , they are the integrated entropy flow, the entropy exchanged between the reaction vessel and the surroundings.  $^{61}$ 

#### C. Dynamic scaling ansatz

To characterize the statistical evolution of an ensemble of M statistically independent trajectories, we analyze the average,  $h_A(N,t) = \langle A(N,t) \rangle = M^{-1} \sum_x^M A(x,N,t)$  using  $M=10^4$  for each chosen observable, A. We quantify fluctuations about this mean across the trajectory ensemble using the variance

$$w_A^2(N,t) = M^{-1} \sum_{x}^{M} \left[ A(x,N,t) - h_A(N,t) \right]^2,$$
 (6)

which depends on time and the number of N molecules in the volume V at t = 0. Our objective here is to analyze the dynamic scaling of the mean and the variance for observables of the stochastic dynamics of chemical systems. This scaling is analogous to the roughening of surfaces, as illustrated in Fig. 1. Each panel in Fig. 1(a) shows the value of the dynamical activity across an ensemble of trajectories. This perspective of the ensemble shows an

abstract "surface" whose dynamic behavior is governed by stochastic trajectories of a unimolecular decay process,  $A \to B$ . In this analogy,  $h_A(N,t)$  and  $w_A^2(N,t)$  are the average height and interfacial width, respectively, that lead to scaling relationships and chemical universality classes.

For a fixed reaction volume that is large compared to molecular length scales, our dynamic scaling ansatz for the mean  $h_A$  and variance  $w_A$  of trajectory-level thermodynamic observables is

$$h_A(N,t) \sim N^{\gamma} f_A[(\kappa t)^{\delta} N^{\zeta}]$$

$$w_A^2(N,t) \sim N^{\gamma} g_A[(\kappa t)^{\delta} N^{\zeta}].$$
(7)

The scaling functions of the mean  $f_A$  and the variance  $g_A$  are different in most of the reactions we consider, but all the reactions have three characteristic exponents. The three scaling exponents are as follows:

- (i) The wandering exponent γ is a measure of the self-averaging property<sup>63</sup> of the observable, A. A γ > 0 implies that the relative variance of A decays as w<sub>A</sub><sup>2</sup>/h<sub>A</sub><sup>2</sup> ~ N<sup>-γ</sup> with increasing numbers of molecules for all times. Most, but not all, of the observables we consider here are system-size extensive with γ = 1 for their mean and their variance. Observables that are system-size intensive and self-average, however, will have a wandering exponent of 0 for their mean and -1 for their variance.
- (ii) The *dynamic exponent*  $\zeta$  is specific to the chosen reaction. For a given reaction, we define a characteristic timescale as the time between reaction events:  $t_c := N/\sum_j a_j(t_0)$  with the total propensity  $N^{-1}\sum_j a_j(t_0)$  per molecule. This exponent determines the system size dependence of the characteristic time  $t_c \sim 1/\kappa N^{\zeta}$ . For mechanisms with any number of reactions, the exponent is  $\zeta = b 1$  provided they have the same molecularity b. The value of  $\zeta$  is the same for both mean and variance. When  $t \approx t_c$ ,  $f_A \sim \mathcal{O}(1)$  and  $g_A \sim \mathcal{O}(1)$  so that  $h_A(N, t_c) \sim N^{\gamma}$  and  $w_A^2(N, t_c) \sim N^{\gamma}$ . The dynamic exponent  $\zeta$  accounts for the system size dependence of the time between reaction events; increasing N decreases the time between reactions.

The parameter  $\kappa$  is a constant specific to the particular reaction that makes  $t/t_c = \kappa t N^{\zeta}$  dimensionless (see the Appendix). For example, it is the stochastic rate constant  $\kappa = c$  in the case of unimolecular decay, A  $\xrightarrow{c}$  B.

(iii) The growth exponent  $\delta$  determines the power law growth of the scaling functions. We find  $f_A$  and  $g_A$  for the mean and variance go as  $(\kappa t)^{\delta}$  for the activity,  $-Q_+$ , and  $-Q_-$ . These scaling functions hold at all times for reactive systems at equilibrium and nonequilibrium stationary states and at early times for systems transiently relaxing to stationary states. The well-mixed chemical systems here all have  $\delta=1$  for the mean and variance, reflecting initial Poisson growth.

We have examined this scaling ansatz for reactive systems at equilibrium, transiently relaxing to equilibrium, and at nonequilibrium steady-state. It holds for K,  $Q_+$ ,  $Q_-$ , and under some circumstances for  $Q_s$ . Moreover, we find from our simulation data that

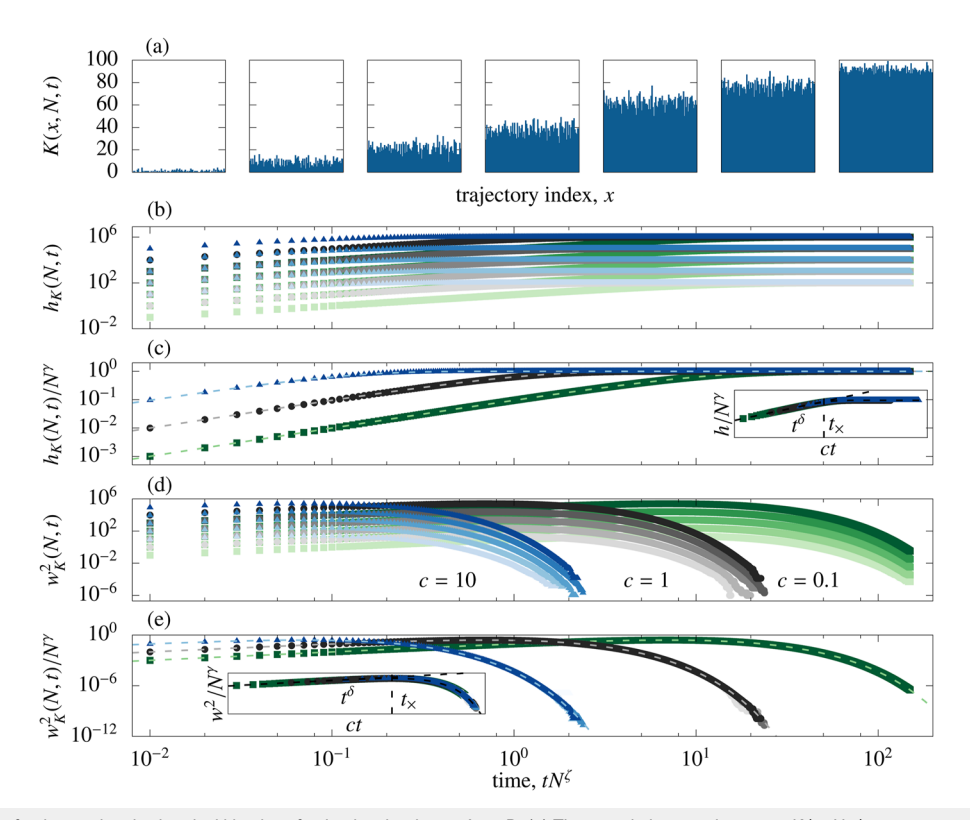


**FIG. 1.** Dynamic scaling for the stochastic chemical kinetics of unimolecular decay,  $A \to B$ . (a) The cumulative reaction count K(x,N,t) across a representative ensemble of simulated trajectories at seven different times, t=0.1,1,2.5,5,10,15,25 in 1/c units. Mean,  $h_K(N,t)$ , and variance in the reaction count,  $w_K^2(N,t)$ , grow as  $t^\delta$  with  $\delta=1$  up to the crossover at time  $t_\times=c^{-1}\ln 2$  after which the mean saturates and the variance decay to zero. For a given c, data for the (b) mean activity as a function of time collapse onto a single curve when (c) scaled by system size  $h_K(N,t)/N^\gamma$  with  $\gamma=1$ . For a given c, data for the (d) variance  $w_K^2(N,t)$  as a function of time also collapse onto a single curve when (e) scaled  $w_K^2(N,t)/N^\gamma$  by the system size with  $\gamma=1$ . Time is scaled  $t\to tN^\zeta$  and for this unimolecular reaction the dynamic exponent is  $\zeta=0$ . Points are numerical data, and dashed lines are from the analytical expression. Colors indicate  $\kappa=c=0.1$  (green), 1.0 (black), and 10.0 (blue) with darker colors indicating larger  $N(N=10^2-10^6$  molecules). Insets in (c) and (e) show that scaling time by c collapses data for all rate constants.

the exponents  $\gamma$ ,  $\zeta$ , and  $\delta$  are related through  $\gamma/\delta = \zeta - b + 2$ . For bimolecular reaction systems, this scaling relation becomes  $\zeta = \gamma/\delta$ , which is similar to the Family–Vicsek scaling law in surface roughening,  $z = \alpha/\beta$ .

## III. SINGLE MOLECULARITY CHEMICAL REACTIONS A. Irreversible decay

As an illustration of the scaling ansatz, consider the irreversible reaction  $A \xrightarrow{c} B$  in a closed reaction volume. Initially, the vessel contains only A and at a sufficiently long time later, it contains only B. We chose these stochastic kinetics because they are both analytically and numerically solvable (Fig. 1). This reaction is an event-modulated Poisson process with a propensity  $a(X \to X + v, t) = cX_A(t)$  that decreases over time. At early times, we find both the mean and variance in the activity grow as the mixture, initially all reactant, becomes more chemically heterogeneous, Fig. 1. But at long times, as the population of A is depleted, the mean saturates and the variance is suppressed.

Statistical correlations in the activity across the trajectory ensemble are the mechanism generating the onset of a new regime

of behavior [Fig. 1(a)]. The correlations are apparent in  $h_K$  and  $w_K^2$ ; they are caused by the irreversibility of the reaction and the conserved number of molecules N. As shown in Figs. 1(b) and 1(d), the mean and variance of the activity go as  $h_K \sim N^{\gamma} t^{\delta}$  and  $w_K^2 \sim N^{\gamma} t^{\delta}$ , respectively. Scaling  $h_K \to h_K/N^{\gamma}$  and  $w_K^2 \to w_K^2/N^{\gamma}$  gives data collapse with  $\gamma = \delta = 1$ ,  $\zeta = 0$  for a given stochastic rate constant c [Figs. 1(c) and 1(e)]. Our numerical data agrees with the exact expression for the mean activity,  $h_K(N, t) = N(1 - e^{-ct})$ , which goes as  $Nct^1$  when  $t \ll c^{-1} \ln 2$  and saturates at N when  $t \gg t_{\times} = c^{-1} \ln 2$  [Fig. 1(b)]. While the nature of the correlations is different, the result is reminiscent of ballistic deposition where the interfacial width saturates because of lateral correlations that develop from finite system size and irreversible particle deposition.1 Unlike physical roughening, the late time behavior in this reaction process is smoothing instead of constant roughness.

The variance in the dynamical activity from numerical simulations also agrees with the exact expression,  $w_K^2(N,t) = Ne^{-ct}(1-e^{-ct})$  [Fig. 1(d)]. Using  $e^{-ct} = 1-ct + \mathcal{O}(ct)^2$  for  $ct \ll 1$ , there is power law growth  $w^2(N,t)/N^{\gamma} \sim (ct)^{\delta}$  with  $\delta = 1$ . Fluctuations, as measured by the variance, grow to the value

 $w^2(N, t_{\times}) = N/4$  at the crossover time  $t_{\times} = c^{-1} \ln 2$ , after which they die out. The scaling function is

$$g_{K}^{A \to B} = e^{-ct} (1 - e^{-ct}) \sim \begin{cases} (ct)^{\delta} & \text{if } t < t_{\times} \\ \frac{1}{4} & \text{if } t = t_{\times} \\ e^{-ct} & \text{if } t > t_{\times}. \end{cases}$$
(8)

Altogether, from our exact expressions and numerical data, the mean and variance of the dynamical activity K are both system size extensive such that  $\gamma = 1$ . With the molecularity b = 1, the exponential arguments above give  $\zeta = 0$ , and the scaling functions initially grow as  $t^{\delta}$  with  $\delta = 1$  up to the crossover time  $t_{\times} = c^{-1} \ln 2$ .

For this reaction, we have focused on the dynamical activity because its mean and variance as a function of time can be found analytically. The scaling exponents follow immediately from the exact expressions for  $h_k$  and  $w_K^2$ . However, because there are only  $A \to B$  transitions, the observables  $Q_+$  and  $Q_s$  are less useful. There is no branching along stochastic trajectories, only one path is possible, and the only randomness is in the stochastic time sequence of  $A \to B$  events; hence,  $Q_+$  is zero for all times. Because of the irreversibility of this reaction,  $Q_-$  is undefined. The entropy flow  $Q_s$  diverges because of the violation of detailed balance<sup>41</sup> at the stationary state. However, these observables are still of interest for larger reaction mechanisms, provided the mechanism supports a stationary state with detailed balance.

To test our scaling ansatz further, we considered sets of unimolecular reactions that are coupled in serial [Figs. 2(a) and 2(c)] and parallel [Figs. 2(b) and 2(d)]. The scaling ansatz in Eq. (7) holds for both cases yielding the scaling exponents  $(\gamma, \delta, \zeta) = (1, 1, 0)$ . We then hypothesize that the dynamic scaling ansatz in Eq. (7) holds for the dynamical activity of any unimolecular, irreversible reaction, regardless of the molecular nature of the reactant A or product B and the connectivity of the reaction network.

With the dynamical activity, this example of unimolecular decay also illustrates another layer of universality. When the reaction vessel is thermostatted, the stochastic rate constant in  $t_c$  is a function

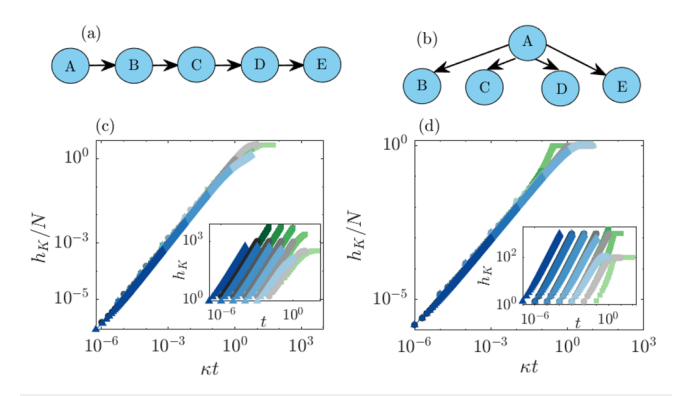


**FIG. 2.** Effect of connectivity of reactions on the scaling function of unimolecular reactions. Schematics of reaction network where the reactions are coupled in (a) serial and (b) parallel. (c) Scaling the mean  $h_K(N,t)/N^{\gamma}$  and time  $t/t_c = \kappa t N^{\zeta}$  collapses data at all times when reactions are coupled in (c) serial (d) parallel. Insets shows the raw data. In all cases, c = 1/10 (green), 1 (black), and 10 (blue) and  $N = 10^2$ ,  $10^3$ ,  $10^4$ ,  $10^5$ , and  $10^6$ .

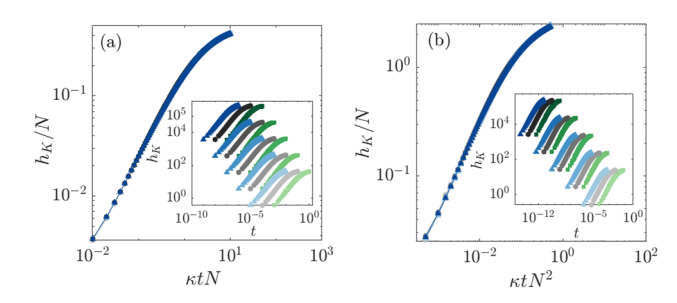


**FIG. 3.** Dynamic scaling for the stochastic chemical kinetics of bimolecular  $A+B\to C+D$  and termolecular  $A+B+C\to D+E+F$  decay processes. (a) The mean activity of the bimolecular reaction collapses onto a single curve when scaled by system size  $h_K(N,t)/N^\gamma$  with  $\gamma=1$  and time  $t/t_c=\kappa tN^\zeta$  with  $\zeta=1$ . (b) The mean activity of the termolecular reaction collapses onto a single curve when scaled by system size  $h_K(N,t)/N^\gamma$  with  $\gamma=1$  and time  $t/t_c=\kappa tN^\zeta$  with  $\zeta=2$ . Insets shows the raw data. In all cases,  $\kappa=c=1/10$  (green), 1 (black), and 10 (blue) and  $N=10^2$ ,  $10^3$ ,  $10^4$ ,  $10^5$ , and  $10^6$ .

of temperature,  $\kappa = c(T)$ . Scaling time  $t \to t/t_c = \kappa t N^{\zeta}$  by the characteristic time,  $1/cN^{\zeta}$ , gives further data collapse of the variance in activity at different temperatures [Fig. 1 (insets) and Figs. 2(c) and 2(d)]. Therefore, we can hypothesize that not only does the dynamic scaling ansatz in Eq. (7) hold for any unimolecular, irreversible reaction regardless of the nature of A and B, it also holds for these reactions in a container at any temperature.

To extend the scaling ansatz to reactions of different molecularity, we considered the bimolecular  $A+B\to C+D$  and termolecular  $A+B+C\to D+E+F$  decay processes shown in Figs. 3(a) and 3(b), respectively. We see good data collapse for the mean activity of the bimolecular reaction with scaling exponents  $(\gamma, \delta, \zeta) = (1, 1, 1)$ . For the termolecular reaction, the scaling exponents are  $(\gamma, \delta, \zeta) = (1, 1, 2)$ . These data suggest that any well-mixed elementary chemical reaction of the form  $\sum_k v_k X_k \to \sum_k v_k Y_k$  obeys the scaling ansatz with the scaling exponents  $(\gamma, \delta, \zeta) = (1, 1, b-1)$  that are determined by the molecularity of the reaction, b.

#### B. Reversibility, molecularity, and reaction conditions

We sought to test the ansatz more generally for chemical reactions beyond irreversible decay. To start, we systematically varied the main features of the chemical mechanism and the reaction conditions, analyzing reactions both at and away from equilibrium. For larger mechanisms, we found that the scaling ansatz holds for any set of reactions, regardless of whether the reactions are coupled in serial or in parallel or consist of cycles when the mechanism is composed of elementary reactions with the same molecularity.

One class of reactions we considered was reversible elementary reactions at equilibrium. Any elementary chemical reaction of the form  $v_WW + v_XX + \cdots = v_YY + v_ZZ + \cdots$  obeys the scaling ansatz and has the scaling exponents  $(y, \delta, \zeta) = (1, 1, b - 1)$  (Fig. 4), provided the forward and reverse reactions have the same molecularity, b. Here,  $v_X$  represents the stoichiometric coefficient of chemical species X. For example, A = B at dynamic equilibrium has a mean and variance that agree with our scaling hypothesis for K,  $Q_+$ , and  $Q_-$ . Here, dynamic equilibrium is the state in which the forward and reverse reaction rates are equal and the composition of the system is unchanging. We confirmed the agreement both

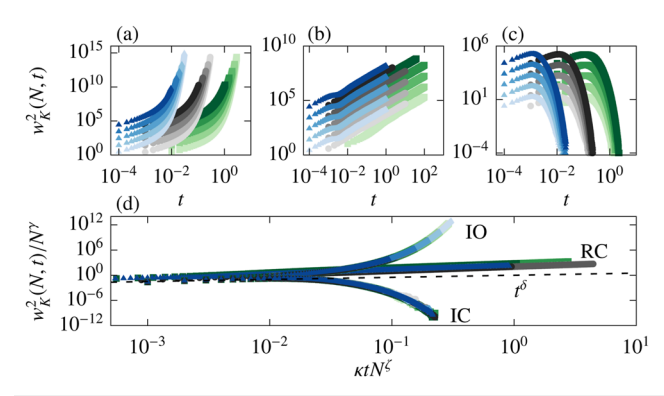


**FIG. 4.** Effect of experimental conditions and the reaction reversibility on the scaling function of a bimolecular, autocatalytic reaction. The variance of the activity  $w_K^2(N,t)$  as a function of time when the reaction is (a) irreversible in a vessel that is open  $\overline{A}$  + B  $\rightarrow$  2B (IO), (b) reversible in a closed reaction vessel and at dynamic equilibrium, A + B  $\rightleftharpoons$  2B (RC), and (c) irreversible in a closed vessel A + B  $\rightarrow$  2B (IC). In all cases, c = 1/10 (green), 1 (black), and 10 (blue), with a reverse rate constant of one for RC conditions and N = 10², 10³, 10⁴, 10⁵, and 10⁵. (d) Scaling the variance  $w_K^2(N,t)/N^\gamma$  and time  $t/t_c = \kappa tN^\gamma$  collapses data at all times. The scaling function  $g_K$  depends on both the reaction reversibility and molecularity and the experimental conditions, behaving as  $g_K \sim t^\delta$  at all times for RC conditions and at early times otherwise.

analytically and numerically. As shown in Fig. 5, the mean and variance of the branching observables diverge as  $h_Q(N,t) \sim N^{\gamma} t^{\delta}$  and  $w_Q^2(N,t) \sim N^{\gamma} t^{\delta}$ , respectively. Also of note is that the scaling ansatz in Eq. (7) for the standard deviation give  $\delta = 1/2$ , which agrees with growth exponent in the random deposition model, the Gaussian universality class.

Another group of reactions that agree with the scaling ansatz are irreversible reactions. We considered irreversible reactions of the form  $\sum_i v_i \overline{W}_i + \sum_j v_j X_j + \cdots \rightarrow \sum_k v_k Y_k + \sum_l v_l Z_l + \cdots$ , where  $\overline{W}_i$  indicates a molecular population that is constant over time (for a particular N) because it is in excess or because of the permeability of the vessel walls to a reservoir of  $W_i$ . The molecular population of  $W_i$  may change when varying the total number of molecules N, since the total molecular number is the sum of the molecular populations of all species. For this class of reactions, the scaling exponents for the mean and the variance of K are  $(\gamma, \delta, \zeta) = (1, 1, b - 1)$ .

Autocatalytic reactions are particularly important in combustion and the chemistry of living systems. Well-mixed reactions of the form  $X_i \rightarrow n'X_i$  with branching coefficient n' (supplementary material, Fig. 1) also agree with the scaling ansatz. Entire cycles of autocatalytic reactions do as well, such as the stochastic Hinshelwood cycle for cell division (supplementary material, Fig. 2). Iyer-Biswas et al. showed the statistics of the copy numbers and division times obey complementary scaling laws. For an individual autocatalytic reaction in the cycle,  $X \rightarrow 2X$ , we found our scaling ansatz holds for the mean  $h_K(N,t) = Ne^{ct}$  and the variance in dynamical activity  $w_K^2(N,t) = Ne^{+ct}[e^{+ct} - 1]$ , which grows as  $t^{+1}$  at short times and as  $e^{2ct}$  at long times, in agreement with numerical simulations.

From this survey of reactions, as we found for unimolecular decay, the scaling exponents and scaling functions depend on both

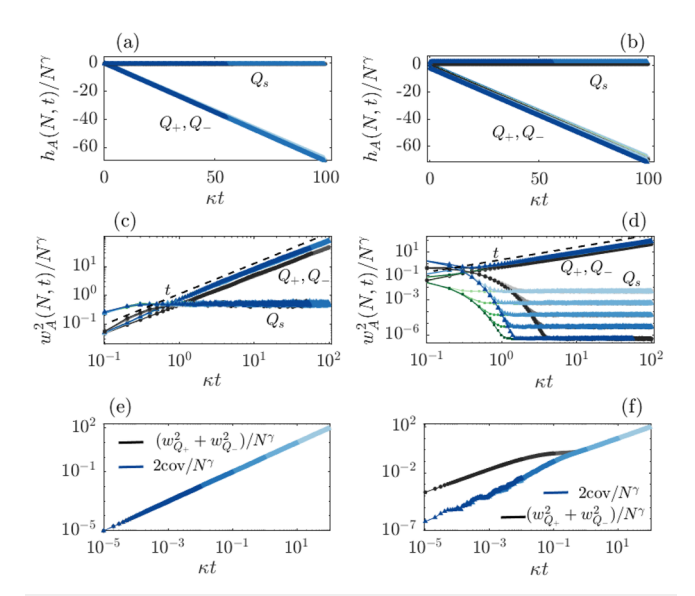


FIG. 5. Confirmation of dynamic scaling ansatz for the thermodynamic branching observables  $Q_+$ ,  $Q_-$ , and the entropy flow  $Q_s = Q_+ - Q_-$  for a reaction mixture at equilibrium and relaxing to equilibrium in a closed reaction vessel. The reversible reaction  $A \rightleftharpoons B$  occurs [(a), (c), and (e)] at equilibrium and [(b), (d), and (f)] relaxing to equilibrium from an initial state of all A molecules. Mean  $h_Q(N,t) \sim N^\gamma t^\delta$  of the branching observables  $Q_+$ ,  $Q_-$ , and  $Q_s$  as a function of time (a) at equilibrium and (b) relaxing to equilibrium. Corresponding variance  $w_Q^2(N,t) \sim N^\gamma t^\delta$  as a function of time (c) at and (d) relaxing to equilibrium. In (a)–(d), the forward rate constant is  $c_f = 0.1$  (green), 1 (black), and 10 (blue); the reverse rate constant is [(a) and (c)]  $c_r = c_f$  and [(b) and (d)]  $c_r = 1$ . Darker colors indicate larger  $N: N = 10^2 - 10^6$ . (e) Sum of variances,  $w_{Q_+}^2 + w_{Q_-}^2$ , and  $cov(Q_+, Q_-)$  (e) at equilibrium (f) relaxing to equilibrium from an initial state of all reactant. In (e) and (f),  $c_f = c_r = 1$ . The wandering exponent is  $\gamma = 1$  for the mean of  $Q_{+/-}$  and the variance  $w_Q^2 \sim N^{+1}t^{+1}$ . At equilibrium,  $Q_s$  has a scaling exponent  $\gamma = 0$  both for its mean and variance. During the relaxation to equilibrium and  $\gamma = 0$  near equilibrium.

the nature of the chemical reaction (reversibility, molecularity) and the chosen experimental reaction conditions (open, closed). When density is fixed instead of volume, the scaling exponents are the same regardless of the molecularity of the reaction or the conditions  $(\gamma, \delta, \zeta) = (1, 1, 0)$ .

In our analysis of these reactions, we also scaled the time coordinate by the parameter  $\kappa$  to achieve data collapse for different choices of rate constants. For single, reversible reaction systems that conserve the total number of molecules, we determined  $\kappa$  as described in the Appendix. Scaling time by  $\kappa$  collapses the distribution of waiting-times between reaction events; for single-reaction systems, the mean and variance of an observable A for reactions with different rate constants collapse onto a single curve. So, the systemsize intensive parameter  $\kappa$  is defined such that  $\kappa t$  is a dimensionless time but also such that the scaling functions  $f_A$  and  $g_A$  are independent dent of the stochastic rate constants of the forward,  $\vec{c_f}$ , and reverse,  $c_r$ , reactions. Figures 4 and 5 show that with  $\kappa$ , the scaling functions of  $h_A$  and  $w_A^2$  for different  $c_f$  and  $c_r$  collapse onto a single curve, independent of the identity of the chemical species and the rate constants governing the reactions. The values of the rate constants are commonly taken to be functions of temperature through an

**TABLE I.** Scaling exponents for the dynamical activity, *K*, in the reaction mechanisms considered here.

Reaction	γ	δ	ζ
Unimolecular <sup>a</sup>	1	1	0
Bimolecular <sup>b</sup>	1	1	1
Termolecular <sup>c</sup>	1	1	2
Mixed molecularity 1 <sup>d</sup>	1	1	1
Mixed molecularity 2 <sup>e</sup>	1	1	0

 $<sup>^{</sup>a}A \rightarrow B$  in a closed container,  $\overline{A} \rightarrow B$  open to A, A  $\rightleftharpoons$  B at and relaxing to equilibrium, A  $\rightarrow$  2A autocatalytic reactions, A  $\rightarrow$  B  $\rightarrow$  C  $\rightarrow$  D  $\rightarrow$  E reactions coupled in serial and A  $\rightarrow$  B, A  $\rightarrow$  C, A  $\rightarrow$  D, A  $\rightarrow$  E in parallel.

Arrhenius expression. Within this modeling assumption, these scaling functions do not depend on the chemical species or temperature.

Table I summarizes the reaction mechanisms and dynamic scaling exponents for the activity, K, that we considered here.

#### C. Dynamic scaling of entropy

More observables satisfy this ansatz than the data shown so far would suggest. We also analyzed the scaling of the path observables relating to entropy:  $Q_+$ ,  $Q_-$ ,  $Q_s$ , and  $\Delta s_i$ .

#### 1. Information-theoretic entropy rates

For reactions where there is branching, the scaling exponents, function, and relation of  $-Q_+$  and  $-Q_-$  are the same as those of cumulative reaction count. The observables K,  $Q_+$ , and  $Q_-$  are extensive, and so,  $(\gamma, \delta, \zeta) = (1, 1, b - 1)$ . For chemical reactions that are well described by Poisson processes, we can relate the scaling of  $Q_+$  and  $Q_-$  to another entropy, the entropy per unit time, <sup>52,62</sup> and determine the scaling exponents exactly. While this entropy rate has previously been used to extract typical paths in nonequilibrium chemistry, <sup>67</sup> its scaling has not been investigated.

As an example, take the equilibrium reaction A = B and assume the propensities are constant and proportional to the mean number of molecules of A and B. In that case, we find from the thermodynamic formalism of Markov processes<sup>52</sup> that the entropy rate is  $-\langle Q_+ \rangle/t = h_{KS} = (a_f + a_r) \ln[(a_f + a_r)/a_f]$ . To make this result more transparent, consider  $c_f = c_r = 1$  with  $a_f = X_A^{eq}$  and  $a_r = X_B^{eq}$ . With these values the entropy per unit time  $h_{KS} = N \ln N /$  $X_A = N \ln 2$  is extensive in system size and the branching observable  $\langle Q_+ \rangle = -Nt \ln 2$  is extensive in system size and time. A similar result holds for Q<sub>-</sub>. For both branching observables, the mean has the scaling exponents  $(\gamma, \delta, \zeta) = (1, 1, 0)$ . From the thermodynamic formalism, we also find the exact scaling exponents for the variance  $w_Q^2(N,t) = t(a_f + a_r) \ln[(a_f + a_r)/a_f]$ . Again assuming that  $c_f = c_r = 1$ , the variances for both  $Q_+$  and  $Q_-$  are  $Nt \ln(N/X_A)$ =  $Nt \ln 2$ . The variance of the branching observable  $w_Q^2/N^{\gamma}$  then grows as t and  $w_0^2/Nt = \ln 2$ . For both branching observables then, the mean and variance have the scaling exponents  $(\gamma, \delta, \zeta)$  = (1, 1, 0). These analytical predictions agree with our numerical data as shown in Fig. 5.

#### 2. Entropy flow

The branching observables  $Q_+$  and  $Q_-$  evolve at an entropy (rate) and are related to the entropy production and flow. At the ensemble level, the entropy that flows between the reaction vessel and the surroundings as the system evolves is related to  $Q_s = Q_+ - Q_-$  through  $\langle Q_s \rangle = -\Delta S_e$ . The entropy flow for A = B is shown in Figs. 5(a) and 5(c) at equilibrium and Figs. 5(b) and 5(d) relaxing to equilibrium from an initial population of pure reactant A. For all the reactions and nonequilibrium initial conditions we consider, the mean entropy flow has a  $\gamma = 1$  for all times, regardless of whether the system is away from equilibrium or relaxed to equilibrium [Fig. 5(b)]. The entropy flow, however, is a cumulative quantity and reflects the path and initial conditions; when the mixture is at equilibrium for all times, the mean entropy flow is zero and scales as  $N^0$ , Fig. 5(a).

Unlike the other observables we consider, the wandering exponent  $\gamma$  for the variance of the entropy flow varies in time as reaction mixtures relax to equilibrium. At  $t=t_0$ , we find good data collapse with  $\gamma=1$  for  $h_{Q_s}$  but also  $w_{Q_s}^2(t_0)\sim N^{+1}$  [Fig. 5(d)]. The relative variance  $w_{Q_s}^2/h_{Q_s}^2$  scales as  $\sim N^{-1}$ , so the entropy flow (and the heat, assuming local detailed balance) is strongly self-averaging. As the system evolves from pure reactant A through successive nonequilibrium states to equilibrium proportions of A and B, the variance of the entropy flow transition from  $\gamma=1$  to  $\gamma=0$  [Figs. 5(b) and 5(d)].

The variance in the entropy flow (and production) exhibit an even richer scaling behavior that depends on the scaling of correlations between  $Q_+$  and  $Q_-$ . For the reactions above that are in detailed balance, the variance  $w_{Q_s}^2 \sim N^0$  satisfies our scaling ansatz with y=0 [Fig. 5(c)]; it is independent of the system size N. While spatial correlations manifest at critical points, here the correlations are temporal correlations between the forward and conjugate reverse paths.

The distinct scaling behavior of  $w_{Q_s}^2$  at and during the relaxation to equilibrium is the result of (positive) correlations between  $Q_+$  and  $Q_-$  (Fig. 5). Because  $Q_s$  is the sum of two potentially correlated variables  $Q_+$  and  $-Q_-$ , its variance is  $w_{Q_s}^2 = w_{Q_+}^2 + w_{Q_-}^2 - 2[\langle Q_+Q_-\rangle - \langle Q_+\rangle\langle Q_-\rangle]$ . The transition of the wandering exponent  $\gamma$  from one to zero is understandable from the limiting cases. As shown in Figs. 5(b) and 5(d), the reactant A is initially in excess, so early in the relaxation process the reaction is effectively the decay from pure A and reaction events are predominantly  $A \to B$ . As shown in Sec. III A, this reaction has  $(\gamma, \delta, \zeta) = (1, 1, 0)$ . In that case, the  $Q_+$  and  $Q_-$  are uncorrelated or weakly correlated,  $w_{Q_+}^2 + w_{Q_-}^2 \gg 2[\langle Q_+Q_-\rangle - \langle Q_+\rangle\langle Q_-\rangle]$ , and the variance scales as  $w_{Q_s}^2 \approx w_{Q_+}^2 + w_{Q_-}^2 \sim N^{+1}$  [Fig. 5(f)].

By contrast, there is no net preference for forward or reverse

By contrast, there is no net preference for forward or reverse reaction events at chemical equilibrium. Any imbalance created by a forward (reverse) reaction event is soon rectified by a reverse (forward) reaction event; if a forward reaction event occurs, there is a contribution of +q to  $Q_s$  and an increase in  $X_B$ , but this increase in  $X_B$  also increases the reverse propensity, making a subsequent reverse reaction more likely to make a canceling contribution -q to  $Q_s$ . At long times then, when mixtures relax to equilibrium, there are strong correlations between forward and reverse reaction

 $<sup>^{</sup>b}$ A + B → C + D, A + B → 2B in a closed container,  $\overline{A}$ + B → 2B open to A, A + B  $\rightleftharpoons$  2B (equilibrium as well as relaxation process).

 $<sup>^{</sup>c}A + B + C \rightarrow D + E + F$  in a closed container.

<sup>&</sup>lt;sup>d</sup>A + B → 2B, B → C ( $a_1 > a_2$ ), Keizer reaction A + B  $\rightleftharpoons$  2B, B  $\leftrightharpoons$  C ( $a_1, a_2 > a_3, a_4$ ) in Sec. IV.

 $<sup>^{</sup>e}$ A + B → 2B, B → C ( $a_1 < a_2$ ), Keizer reaction A + B  $\rightleftharpoons$  2B, B  $\leftrightharpoons$  C ( $a_1, a_2 < a_3, a_4$ ) in Sec. IV.

events,  $w_{Q_+}^2 + w_{Q_-}^2 \approx 2\text{cov}(Q_+, Q_-) \sim N^{+1}$  and  $w_{Q_i}^2 \sim N^0$  [Figs. 5(c) and 5(e)].

For all reactions and experimental conditions that we consider, we find the means  $\langle Q_+ \rangle$ ,  $\langle Q_- \rangle$ , and  $\langle Q_s \rangle$  (away from equilibrium), the variances  $w_{Q_+}^2$  and  $w_{Q_+}^2$ , and the covariance  $\text{cov}(Q_+,Q_-)$  all go as  $\sim N^{+1}$  at all times. However, the magnitude of the (positive) correlations between  $Q_+$  and  $Q_-$  determine the system-size dependence of the entropy flow  $Q_s$  variance. During relaxation processes, as the reaction progress towards equilibrium, these correlations increase as the nonequilibrium currents vanish and the wandering exponent  $\gamma$  varies from 1 to 0.

#### 3. Entropy production

For reactions at equilibrium and nonequilibrium steady-states, the scaling behavior of the entropy production is identical to that of the entropy flow; as can be seen from Eq. (3), they are equal up to a sign under these conditions. For mixtures at chemical equilibrium, we found the scaling exponents and the scaling function are the same for  $\Delta s_e$  and  $\Delta s_i$ . We first confirmed this by considering a reaction vessel that is open reservoirs of A and B molecules, which can transform reversibly  $A \rightleftharpoons B$ . We set  $c_f = c_r$  and the numbers of each species at time-independent nonequilibrium values,  $X_A \ne X_B$ .

Given that our dynamic scaling approach applies outside of equilibrium, we also analyzed the scaling of entropy production for transient phenomena. We again considered the relaxation to equilibrium of a reversible reaction,  $A \rightleftharpoons B$ , in a closed reaction vessel. The vessel initially contains pure A, so  $P(\mathbf{X},t_0)=1$ . At a time  $t\gg (c_f+c_r)^{-1}$ , the mixture will reach chemical equilibrium with a stationary probability distribution given by  $P^{\mathrm{eq}}(N,X_A)=(1+c_f/c_r)^{-N}(c_f/c_r)^{X_A}\binom{N}{X_A}$ . <sup>68</sup> Taking  $c_f=c_r$ , the stationary population is  $X_A^{\mathrm{eq}}=N/2$ . Putting these details together with Eq. (3) gives the entropy production for the relaxation process (supplementary material, Fig. 3). The dependence of the logarithm of the ratio of the initial and final probabilities on N is negligibly small compared to  $Q_s$ . The entropy production then has the same scaling function, relation, and exponents in this case.

Table II summarizes the dynamic scaling exponents associated with the path observables related to entropy for different reaction mechanisms and reaction conditions.

#### D. Analogy with kinetic roughening

Stepping back, we can see our approach to the scaling of stochastic thermodynamic observables as analogous to the dynamic scaling of roughening surfaces. Each numerical simulation here provides a stochastic realization of the reaction that we label, x, specifying the "spatial" location on the "surface" at a time t. Over time, the dynamic growth of the observables across the ensemble of trajectories is the "interface," each point on the interface being associated with a different set of time-ordered chemical events. For the "height" at a given point on the surface, we use observables, A(x, N, t), accumulated up to the time t.

**TABLE II.** Dynamic scaling exponents for  $Q_+$ ,  $Q_-$ ,  $Q_s$ , and  $\Delta s_i$  for different mechanisms and reaction conditions.

		$Q_+, Q$	$Q_s$	$\Delta s_i$					
Reaction				Variance			Variance		
			Mean	$t \to 0$	$t \to \infty$	Mean	$t \to 0$	$t \to \infty$	
Unimolecular $A \Leftarrow B$ , equilibrium	γ	1	0	0	0	0	0	0	
	δ	1	0	0	0	0	0	0	
	ζ	0	0	0	0	0	0	0	
Unimolecular A $\rightleftharpoons$ B, relaxation	γ	1	1	1	0	1	1	0	
	δ	1	1	1	0	1	1	0	
	ζ	0	0	0	0	0	0	0	
Bimolecular $A + B \leftrightharpoons C + D$ , equilibrium	γ	1	0	0	0				
	δ	1	0	0	0				
	ζ	1	0	0	0				
Bimolecular A + B $\rightleftharpoons$ C + D, relaxation	γ	1	1	1	0				
	δ	1	1	1	0				
	ζ	1	1	1	0				
Termolecular A + B + C $\rightleftharpoons$ D + E + F, relaxation	γ	1	1	1	0				
	δ	1	1	1	0				
	ζ	2	2	2	0				
Keizer reaction A + B $\rightleftharpoons$ 2B, B $\rightleftharpoons$ C $a_1, a_2 > a_3, a_4$	ν	1	1	1	0				
	δ	1	1	1	0				
	ζ	1	1	1	0				
Keizer reaction A + B $\rightleftharpoons$ 2B, B $\rightleftharpoons$ C $a_1, a_2 < a_3, a_4$	ν	1	1	1	0				
	δ	1	1	1	0				
	ζ	0	0	0	0				

For example, Fig. 1(a) shows the dynamical activity (cumulative number of reactions) for an ensemble of stochastic simulations of unimolecular decay  $A \xrightarrow{c} B$  in a closed container. The mixture evolves to an absorbing state in which only B is in the reaction vessel on a timescale set by the stochastic rate constant  $c^{-1}$ . Here, the value of K(x, N, t) across the ensemble of trajectories is an abstraction of a rough physical surface. The trajectory index corresponds to the "spatial location." An important difference with traditional surface roughening is that here we do not analyze the dependence of the height or width of the interface (mean or variance of the given stochastic thermodynamic quantity) on the length of the surface (the number of trajectories). Instead, we analyze the dependence of these cumulative properties of the xth trajectory,  $A(x, N, t) := A[\hat{\mathbf{X}}_x(t)]$ on the system size (as measured by the total number of molecules).

Taking this analogy a step further for the activity, we can put the scaling relation into the form of the well-known Family-Vicsek relation.  $^{64,69}$  Let the initially N molecules exclude a volume  $L^d$  with d spatial dimensions of length L. We can then define the "roughness" exponent as  $\alpha' := d\gamma$  and dynamic exponent as  $z' := -d\zeta$  such that  $z' \le 0$ ; similar algebraic relationships between the  $\alpha$  and  $\gamma$  are known for Lyapunov exponents.<sup>28</sup> With these definitions, our ansatz takes the Family-Vicsek form:  $h_A(L,t) \sim L^{\alpha'} f_A(\kappa t/L^{z'})$  and  $w_A^2(L,t)$  $\sim L^{\alpha'}g_{\Delta}(\kappa t/L^{z'}).$ 

An important difference with the Family-Vicsek scaling function is that the scaling functions for chemical reactions do not tend to saturate like those in physical surface roughening. This difference is the result of our chosen observables, the reaction mechanisms, and the characteristic timescale, all of which motivate different scaling exponents. The scaling functions  $f_A$  and  $g_A$  depend on both the nature of the chemical reaction (reversibility, molecularity) and the chosen experimental reaction conditions (open, closed) (Fig. 4). As a consequence, the scaling law is  $\alpha'/d\delta = -z' - d(b-2)$ . For bimolecular reaction systems, however, it becomes  $-z' = \alpha'/d\delta$ . This form of the scaling law only differs in sign from that in surface roughening,  $z = \alpha/\beta$ ; the sign difference is the result of the  $N^{-\zeta} = L^{-d\zeta}$ dependence of our timescale  $t_c$  instead of the  $L^z$  dependence of the crossover time used in surface roughening.

#### IV. COUPLED CHEMICAL REACTIONS

The scaling exponents found so far are unaffected by coupling reactions with the same molecularity. However, analyzing two coupled reactions with different molecularity and tuning their irreversibility leads to a collision of universality classes.

#### A. Keizer reaction

Collisions and reactions between four-bodies are sufficiently improbable that they are commonly neglected in chemical kinetics. We then only need to consider the dynamic exponent  $\zeta$  for unimolecular, bimolecular, and termolecular reaction types. From our scaling ansatz, we expect each molecularity involved to have the potential to contribute to a scaled dynamic exponent  $\zeta = b - 1$ when chemical reactions of different molecularity are coupled. In these cases, we do find that additional scaling exponents are generally necessary. Additional exponents can also be necessary in the dynamic scaling of other systems when there is more than one mechanism. 64,69 However, there can be experimental conditions where reactions of a particular molecularity are dominant and a single dynamic exponent  $\zeta$  is sufficient.

As a representative example, we apply our scaling approach to an autocatalytic bimolecular reaction and a unimolecular reaction

$$A + B \stackrel{c_1}{\rightleftharpoons} 2B$$

$$B \stackrel{c_3}{\rightleftharpoons} C.$$
(9)

By altering the rate constants of each elementary reaction, we can tune the (ir)reversibility of the overall reaction. Similar autocatalytic reactions can be found in biochemical reactions, such as the phosphorylation activation of certain enzymes.<sup>7</sup>

As a first example, we considered both reactions in (9) to be purely irreversible (i.e.,  $c_2 = c_4 = 0$ ). For this case, there are two scaling regimes shown in Fig. 6(a). When the propensities of the first and second reaction steps are such that  $a_2 \gg a_1$ , the unimolecular termination reaction dominates the kinetics and there is good data collapse with  $\zeta = 0$  [Figs. 6(b)-6(d)], and when  $a_1 \gg a_2$ , the bimolecular branching reaction dominates the kinetics and there is good data collapse of  $\langle K \rangle / N^{\gamma}$  as a function of  $\kappa t N^{\zeta}$  with a single dynamic exponent  $\zeta = 1$  [Figs. 6(c)-6(e)]. That is, experimental conditions can exist where, despite the existence of two characteristic timescales, one timescale can dominate the kinetics and lead to a single dynamic scaling exponent.

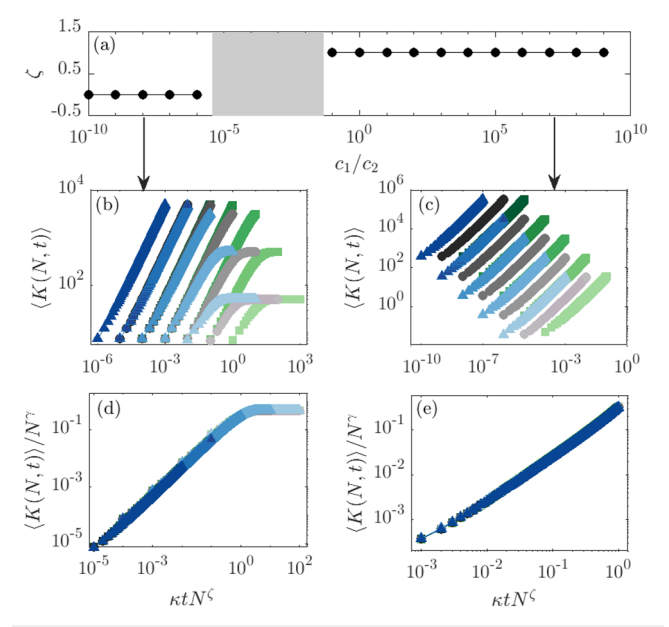


**FIG. 6.** Dynamic scaling for the stochastic chemical kinetics of  $\overline{A} + B \xrightarrow{c_1} 2B$ ,  $B \xrightarrow{c_2} C$  when both reactions are irreversible and the vessel is open to reactant A. (a) Variation of the dynamic exponents as a function of  $c_1/c_2$  with  $c_2 = 1$  and  $N = 10^2 - 10^6$ . (b) The unimolecular reaction dominates the mean activity as a function of time when  $c_1 = 1 \times 10^{-9}$  and  $\kappa = c_2 = 0.1$  (green), 1.0 (black), and 10.0 (blue). Darker colors indicate larger N. (c) The bimolecular reaction dominates the mean activity as a function of time when  $c_2 = 1$  and  $\kappa = c_1 = 0.1$ (green), 1.0 (black), and 10.0 (blue). Data for all system sizes and all rate constants after scaling the mean activity  $\langle K(N,t) \rangle / N^{\gamma}$  and time  $\kappa t N^{\zeta}$  with (d)  $\gamma = 1$ ,  $\zeta = 0$ when  $c_1/c_2$  is less than about  $10^{-5}$  and (e)  $\gamma = 1$ ,  $\zeta = 1$  when  $c_1/c_2$  is greater

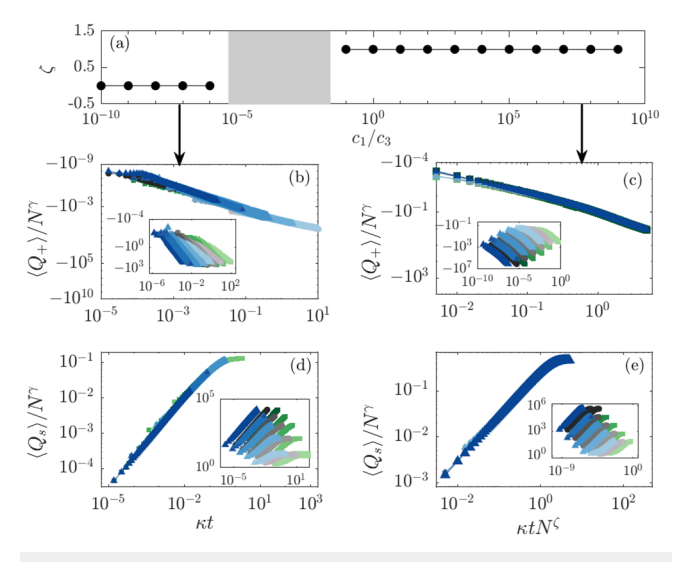


**FIG. 7.** Dynamic scaling for the stochastic chemical kinetics of A + B  $\rightleftharpoons$  2B, B  $\rightleftharpoons$  C in a closed reaction vessel. (a) Scaled dynamic exponent  $\zeta$  as a function of  $c_1/c_3$  transitions from  $0\to 1$ , corresponding to the transition from a unimolecular- to a bimolecular-dominant reaction. Gray region marks where a single  $\zeta$  is insufficient. Here,  $c_1=c_2$  and  $c_3=c_4=1$ . Data collapse for  $\langle Q_+(N,t)\rangle/N^\gamma$  as a function of  $\kappa t N^\zeta$  with (b)  $\zeta=0$  and (c)  $\zeta=1$ . Data collapse for  $\langle Q_s(N,t)\rangle/N^\gamma$  as a function of  $\kappa t N^\zeta$  with (d)  $\zeta=0$  and (e)  $\zeta=1$ . Scaling time by  $\kappa$  collapses data for all rate constants. Insets show raw data as a function of t. (b) and (d) Unimolecular reaction events dominate the kinetics; colors indicate the value of  $\kappa=c_3=c_4=0.1$  (green), 1.0 (black), and 10.0 (blue),  $c_1=c_2=1\times 10^{-9}$ . (c) and (e) Bimolecular reaction events dominate the kinetics; colors indicate the value of  $c_1=c_2=0.1$  (green), 1.0 (black), and 10.0 (blue), and  $c_3=c_4=0.1$ . In all panels,  $N=10^2-10^6$ , with darker colors indicating larger N.

Between these two regimes, the mean thermodynamic observables do not collapse using a single dynamic scaling exponent, and so, they do not satisfy the scaling ansatz [marked gray in Fig. 6(a)]. This regime marks a collision of two classes, here, one with  $\zeta=0$  and another with  $\zeta=1$ . The extent of this region depends on the range of N; the difference between the largest and smallest N is directly proportional to the range of rate constant ratios over which two dynamic scaling exponents are necessary. The largest N determines the  $c_1/c_2$  value up to which unimolecular reaction will dominate, and the smallest N will determine the  $c_1/c_2$  value above which bimolecular reactions dominate. For example, Fig. 6(a) shows that for the ratio of rate constants  $c_1/c_2=10^{-6}$ , when the range of N is  $10^2-10^6$ , only a single exponent,  $\zeta=0$ , is sufficient. Here,  $a_2\gg a_1$  for all N we consider. When  $N=10^2-10^7$ , data collapse is not possible using a single exponent since for  $N=10^7$ ,  $a_1\gg a_2$  and the bimolecular reaction dominates the kinetics.

The dominant molecularity can vary as the reaction progress, which affect the scaling we consider here. For example, in the case where both steps in reaction (9) are irreversible and the second step is rate limiting, then the bimolecular reaction dominates the scaling behavior at early times and the unimolecular reaction dominates at later times. As the reaction progress, there is then a transition between the molecularity defining the dynamic exponent  $\zeta$  in the scaling ansatz. Recognizing this situation, we can identify regions

where the rate parameters lead to a single dominant molecularity. By carefully selecting the rate parameters, we can find regimes where one reaction step determines the scaling behavior for all times.

When both reactions are reversible, conditions also exist where reactions of a particular molecularity dominate the kinetics and the relaxation to equilibrium. For the reversible set of reactions [reaction (9)], the unimolecular reaction dominates the scaling when  $c_1/c_2$  is less than about 10<sup>-5</sup>. The unimolecular and bimolecular reactions compete, however, up to  $c_1/c_2$  of around 0.1, where there is a regime in which the bimolecular reaction dominates the scaling. The extent of the region where both reactions must be accounted for in the scaling is the same as that of the irreversible case, again varying with the range of system sizes. We found similar behavior for  $Q_+$  and  $Q_s$  (Fig. 7). Considering the form of  $\kappa$  used for  $A + B \rightleftharpoons 2B$ , one might expect that  $\kappa$  would be a combination of all four rate constants. However, from our analysis we found that  $\kappa = c_1 = c_2$  when the bimolecular reaction dominates and  $\kappa = c_3 = c_4$  when the unimolecular reaction dominates. For this set of reactions, the reaction step with the highest propensity can determine the characteristic rate  $\kappa$ .

At equilibrium, however, a single dynamic exponent is sufficient for data collapse despite the different molecularities. For instance, the set of scaling exponent for  $A+B \rightleftharpoons C$  at equilibrium is  $(\gamma, \delta, \zeta) = (1, 1, 0)$ , Fig. 8. At equilibrium, the propensity of forward and reverse reaction are the same and, as a result, the bimolecular reaction scales as a unimolecular reaction. Our dynamic scaling ansatz is then also valid for mixed molecular reactions at equilibrium.

#### B. Autocatalytic reaction cycle

We now consider a set of reactions that are the simplest example of a "reaction cycle" leading to autocatalysis,

$$A + B \xrightarrow{c_1} C + D$$

$$C + D \xrightarrow{c_2} A + B$$

$$C \xrightarrow{c_3} 2B$$

$$2B \xrightarrow{c_4} C.$$

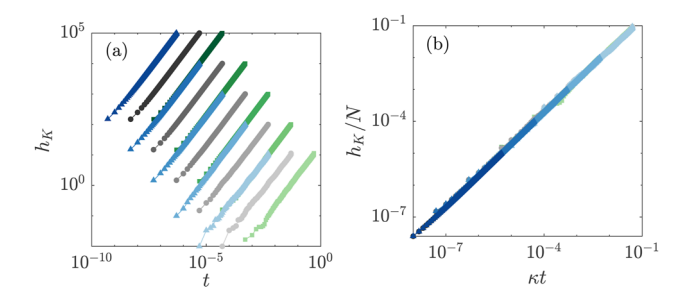


**FIG. 8.** Dynamic scaling function of a mixed molecularity reaction,  $A + B \rightleftharpoons C$ , at equilibrium. (a) The mean activity  $h_K(N,t)$  as a function of time (b) collapses onto a single curve when scaled by system size  $h_K(N,t)/N^y$  with  $\gamma=1$  and time  $t/t_c=\kappa t N^\zeta$  with  $\zeta=0$ . Here,  $c_r=c_f=1/10$  (green), 1 (black), and 10 (blue),  $N_A=N_B=10^1-10^5$ , and  $N_C=N_A^2$ .

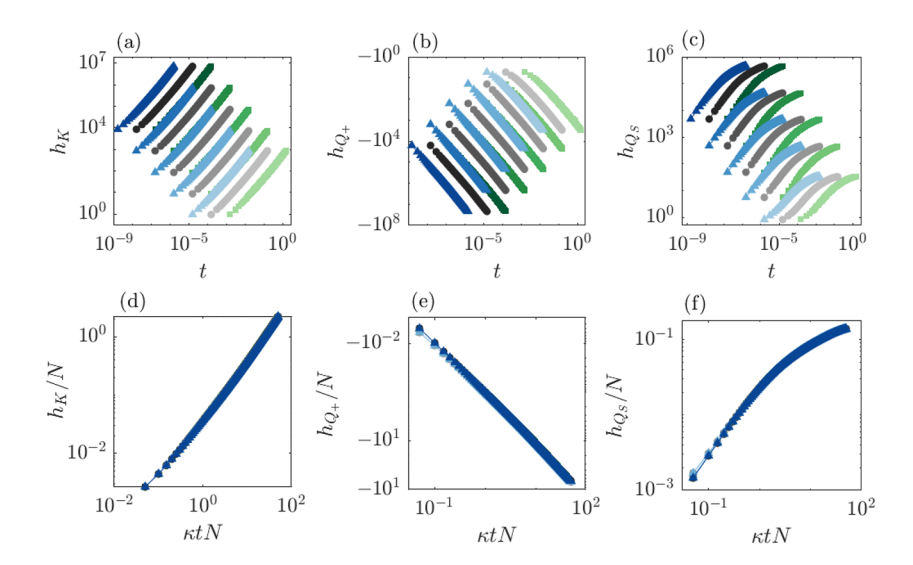


**FIG. 9.** Dynamic scaling for the stochastic chemical kinetics of a random reaction network in a closed reaction vessel. Variation of (a) mean activity  $h_K$ , (b) mean of branching observable  $Q_+$ , and (c) mean of entropy flow  $Q_{\rm s}$  as a function of time. Data collapse for (d)  $h_K/N^{\gamma}$ , (e)  $h_{Q_+}/N^{\gamma}$ , (f)  $h_{Q_s}/N^{\gamma}$  as a function of  $\kappa t N^{\zeta}$  with  $\gamma=1$ ,  $\zeta=1$ . Bimolecular reaction events dominate the kinetics; colors indicate the value of c=0.1 (green), 1.0 (black), and 10.0 (blue). In all panels,  $N=3.25\times 10^2-3.25\times 10^6$ , with darker colors indicating larger N.

The reaction cycle consists of both unimolecular and bimolecular reactions. Bimolecular reactions dominate the kinetics when the reaction propensities satisfy:  $a_3 \ll a_1 + a_2 + a_4$ . To make our results more transparent, we consider the rate constants of all reactions to be identical,  $c_1 = c_2 = c_3 = c_4$ , so that  $a_1, a_2, a_4 \gg a_3$ . Under this condition, we see data collapse with  $\zeta = 1$  for K and  $Q_+$ . We also found that  $\kappa = c$  [supplementary material, Figs. 4(d) and 4(e)].

The scaling for  $Q_s$  is different than that of the activity. The data do not collapse with  $\zeta = 1$  [supplementary material, Fig. 4(f)]. This distinct behavior is a consequence of both forward and backward propensities being involved in the evolution of  $Q_s$ . As a result, the universality classes for  $Q_s$  "collide" despite the clear dominance of the bimolecular reaction in the kinetics. This result can be explained in the following way: When the first (or second) reaction occurs, then the contribution to  $Q_s$  will be  $\approx \ln(N_A N_B/N_C N_D)$  [or  $Q_s \approx \ln(N_C N_D/N_A N_B)$ ]. However, when the fourth reaction occurs, then  $Q_s \approx \ln(N_B (N_B - 1)/N_C)$ . The smaller denominator in the argument of the logarithm will cause a larger contribution to  $Q_s$  compared to cases where all reactions are bimolecular. Hence,  $\zeta = 1$  does not give data collapse, unless we choose particular rate constants. For example, choosing rate constants such that  $c_1 = c_2 \gg c_3 = c_4$ , the data will collapse with  $\zeta = 1$  for  $Q_s$ .

These results demonstrate that for reaction systems with different molecularities, the scaling of  $Q_s$  is more sensitive to the reaction mechanism than the scaling of K or  $Q_+$ . In order to get  $Q_s$  to collapse in systems with reactions of differing molecularity, one molecularity must dominate over others. That is, the rate constants must be such that the reactions of one molecularity exceed those of any other molecularity.

#### C. Random chemical reaction networks

As a final test of the ansatz, we consider the dynamics of many species reaction in a dilute, well-stirred mixture, where species are "wired" together into a chemical reaction network by randomly chosen pairs of species. The network consists of 25 species, interconvertible through one of the 35 reversible reactions. Most of the

reactions in the network are unimolecular (24 out of 35) and the rest are bimolecular. Self-replication is excluded from this reaction mechanism, i.e., no species appear more than once as a reactant or product. We take all rate constants to be the same and break detailed balance by setting the initial numbers of molecules to be different for each species. The initial population of each of 25 species was randomly chosen from the set  $[1, 2, 3, ..., 25] \times N/325$ .

For this reaction network, we get complete data collapse with  $(\gamma, \delta, \zeta) = (1, 1, 1)$  for K,  $Q_+$ , and  $Q_s$ , Fig. 9. Although the probability of bimolecular reactions is 0.3, it still dominates the kinetics over the unimolecular reactions and determines the universality class. Here, a single dynamic exponent is sufficient to get the data collapse even for  $Q_s$  because the molecularity of the forward and the reverse reaction are the same. We can conclude that for a complicated reaction network involving unimolecular, bimolecular, and termolecular reactions, if there is a clear dominance of a particular molecularity at all times, the universality class will be determined by the molecularity of those dominant reactions.

#### V. CONCLUSIONS

While universal behaviors have been extensively explored for physical phenomena, here we have shown that universal dynamical scaling extends to the thermodynamic observables of chemical phenomena at and away from equilibrium. These observables satisfy a dynamic scaling ansatz that we have tested for broad classes of chemistry from simple, elementary reactions to coupled autocatalytic reactions. Dynamical universality classes are typically determined by the dimensionality, conservation laws, symmetry of the order parameter, range of the interactions, and the coupling of the order parameter to conserved quantities. Here, we find classes of well-mixed chemical reactions do not depend on the identities of the chemical species or, in some cases, the temperature fixed by an external bath. Instead, they are determined by the reaction vessel dimensionality, whether the vessel is open or closed, observable extensivity, and reaction molecularity. The ansatz we use to define

these classes include scaling laws and relations, some unknown and some known (Family–Vicsek).

The entropy flow and production have scaling exponents that are different at and away from equilibrium. This difference is the result of correlations between the forward and reverse branching observables as mixtures approach equilibrium. Coupling reactions capable of chemical feedback, creating collections of reactions with multiple molecularities, leads to a richer collection of scaling exponents. In these cases, the variance in thermodynamic observables can transition between these classes with the variation of experimental parameters. We find that despite this behavior, there are conditions where a given molecularity reaction dominates, leading to a single scaling law and universality class. Taking a broad view, while the catalog of chemical reaction mechanisms is incredibly diverse, it does contain universal signatures in their kinetics both at and away from equilibrium.

#### SUPPLEMENTARY MATERIAL

See the supplementary material for additional data.

#### **ACKNOWLEDGMENTS**

The authors acknowledge helpful conversations with Lucas B. Newcomb and the use of the supercomputing facilities managed by the Research Computing Group at the University of Massachusetts Boston as well as the University of Massachusetts Green High Performance Computing Cluster.

This publication was made possible, in part, through the support of a grant from the John Templeton Foundation. It is also based, in part, upon work supported by the National Science Foundation under Grant No. 1856250.

#### **AUTHOR DECLARATIONS**

#### **Conflict of Interest**

The authors have no conflicts to disclose.

#### **Author Contributions**

S.M. and J.S.G. contributed equally to this work.

Shrabani Mondal: Formal analysis (equal); Investigation (equal); Methodology (equal); Software (equal); Validation (equal); Writing – original draft (equal); Writing – review & editing (equal). Jonah S. Greenberg: Formal analysis (equal); Investigation (equal); Methodology (equal); Software (equal); Writing – original draft (equal); Writing – review & editing (equal). Jason R. Green: Conceptualization (lead); Data curation (equal); Funding acquisition (lead); Investigation (lead); Methodology (equal); Project administration (equal); Resources (equal); Supervision (equal); Validation (equal); Writing – review & editing (equal).

#### **DATA AVAILABILITY**

The data that support the findings of this study are available from the corresponding author upon reasonable request.

### APPENDIX: CHARACTERISTIC RATE, $\kappa$ , FOR DETAILED BALANCED SYSTEMS

For single, reversible reaction systems that conserve the total number of molecules, we determined  $\kappa$  using the condition of detailed balance. As an example, take the reversible reaction,

$$A \stackrel{c_f}{\rightleftharpoons} B.$$

The reaction is detail balanced when the forward and reverse propensities are equal:  $c_f X_{\rm A}^{\rm eq} = c_r X_{\rm B}^{\rm eq}$ . When the reaction volume is closed, the total number of molecules is conserved  $N = X_{\rm A} + X_{\rm B}$ . Combined with the detailed balance condition this constraint leads to the equilibrium propensities

$$\frac{a_f^{\text{eq}}}{N} = c_f X_{\text{A}}^{\text{eq}} = \frac{c_f c_r}{c_f + c_r} = c_r X_{\text{B}}^{\text{eq}} = \frac{a_r^{\text{eq}}}{N}.$$
 (A1)

The total propensity per molecule is  $N^{-1}(a_f^{\text{eq}} + a_r^{\text{eq}}) = t_c^{-1} = \kappa N^{\zeta}$  and gives

$$\kappa = \frac{2c_f c_r}{c_f + c_r}.$$
(A2)

Similarly, we found that for bimolecular autocatalytic reaction  $A + B \stackrel{c_r}{\rightleftharpoons} 2B$ ,

$$\kappa = \frac{4c_f^2 c_r}{(c_f + c_r)^2}.$$
(A3)

Through this approach,  $\kappa$  is determined for reactions where detailed balance is satisfied at equilibrium and where we can express the number of each chemical species in terms of N; even for bimolecular reactions  $A + B \leftrightharpoons C$ , this approach does not yield  $\kappa$ .

#### **REFERENCES**

<sup>1</sup> A. L. Barabási and H. E. Stanley, Fractal Concepts in Surface Growth (Cambridge University Press, 1995).

<sup>2</sup>T. Vicsek, Fractal Growth Phenomena, 2nd ed. (World Scientific, 1992).

<sup>3</sup>S. V. Buldyrev, A.-L. Barabási, F. Caserta, S. Havlin, H. E. Stanley, and T. Vicsek, "Anomalous interface roughening in porous media: Experiment and model," Phys. Rev. A **45**, R8313 (1992).

<sup>4</sup>A. S. Balankin, R. G. Paredes, O. Susarrey, D. Morales, and F. C. Vacio, "Kinetic roughening and pinning of two coupled interfaces in disordered media," Phys. Rev. Lett. **96**, 056101 (2006).

<sup>5</sup>A. M. Miranda, I. L. Menezes-Sobrinho, and M. S. Couto, "Spontaneous imbibition experiment in newspaper sheets," Phys. Rev. Lett. 104, 086101 (2010).
 <sup>6</sup>K. A. Takeuchi, M. Sano, T. Sasamoto, and H. Spohn, "Growing interfaces uncover universal fluctuations behind scale invariance," Sci. Rep. 1, 34 (2011).

<sup>7</sup>G. Ódor, "Universality classes in nonequilibrium lattice systems," Rev. Mod. Phys. **76**, 663 (2004).

<sup>8</sup> H. Kim, H. B. Smith, C. Mathis, J. Raymond, and S. I. Walker, "Universal scaling across biochemical networks on Earth," Sci. Adv. 5, eaau0149 (2019).

<sup>9</sup>S. Iyer-Biswas, G. E. Crooks, N. F. Scherer, and A. R. Dinner, "Universality in stochastic exponential growth," Phys. Rev. Lett. **113**, 028101 (2014).

<sup>10</sup>S. Iyer-Biswas, C. S. Wright, J. T. Henry, K. Lo, S. Burov, Y. Lin, G. E. Crooks, S. Crosson, A. R. Dinner, and N. F. Scherer, "Scaling laws governing stochastic

- growth and division of single bacterial cells," Proc. Natl. Acad. Sci. U. S. A. 111, 15912 (2014).
- $^{11}\mathrm{V}.$  Pérez-García, G. Calvo, J. Bosque  $\mathit{et~al.},$  "Universal scaling laws rule explosive growth in human cancers," Nat. Phys. 16, 1232 (2020).
- <sup>12</sup>G. Makey, S. Galioglu, R. Ghaffari et al., "Universality of dissipative selfassembly from quantum dots to human cells," Nat. Phys. 16, 795 (2020).
- <sup>13</sup>T. Halpin-Healy and Y.-C. Zhang, "Kinetic roughening phenomena, stochastic growth, directed polymers and all that. Aspects of multidisciplinary statistical mechanics," Phys. Rep. 254, 215 (1995).
- <sup>14</sup>P. Meakin, "The growth of rough surfaces and interfaces," Phys. Rep. 235, 189
- <sup>15</sup>C.-K. Peng, S. V. Buldyrev, A. L. Goldberger, S. Havlin, F. Sciortino, M. Simons, and H. E. Stanley, "Long-range correlations in nucleotide sequences," Nature 356,
- $^{16}\mbox{B}.$  Barzel and A.-L. Barabási, "Universality in network dynamics," Nat. Phys. 9,
- <sup>17</sup>A. S. Balankin, "Dynamic scaling approach to study time series fluctuations," Phys. Rev. E 76, 056120 (2007).
- <sup>18</sup>Y. Ashkenazy, P. C. Ivanov, S. Havlin, C.-K. Peng, A. L. Goldberger, and H. E. Stanley, "Magnitude and sign correlations in heartbeat fluctuations," Phys. Rev. Lett. 86, 1900 (2001).
- <sup>19</sup> K. Fujimoto, R. Hamazaki, and Y. Kawaguchi, "Family-Vicsek scaling of roughness growth in a strongly interacting Bose gas," Phys. Rev. Lett. 124, 210604
- <sup>20</sup>S. Morel, J. Schmittbuhl, E. Bouchaud, and G. Valentin, "Scaling of crack surfaces and implications for fracture mechanics," Phys. Rev. Lett. 85, 1678 (2000).
- <sup>21</sup> A. S. Pikovsky and J. Kurths, "Roughening interfaces in the dynamics of perturbations of spatiotemporal chaos," Phys. Rev. E 49, 898 (1994).
- <sup>22</sup>A. Pikovsky and A. Politi, "Dynamic localization of Lyapunov vectors in spacetime chaos," Nonlinearity 11, 1049 (1998).
- <sup>23</sup>D. Pazó and J. M. López, "Characteristic Lyapunov vectors in chaotic time-delayed systems," Phys. Rev. E 82, 056201 (2010).
- <sup>24</sup>D. Pazó, J. M. López, and A. Politi, "Universal scaling of Lyapunov-exponent fluctuations in space-time chaos," Phys. Rev. E 87, 062909 (2013).
- <sup>25</sup>M. Kardar, G. Parisi, and Y.-C. Zhang, "Dynamic scaling of growing interfaces," Phys. Rev. Lett. 56, 889 (1986).
- <sup>26</sup>M. Das and J. R. Green, "Self-averaging fluctuations in the chaoticity of simple fluids," Phys. Rev. Lett. 119, 115502 (2017).
- <sup>27</sup>M. Das and J. R. Green, "Critical fluctuations and slowing down of chaos," Nat. Commun. 10, 2155 (2019).
- <sup>28</sup>D. Pazó, J. M. López, and A. Politi, "Diverging fluctuations of the Lyapunov exponents," Phys. Rev. Lett. 117, 034101 (2016).
- <sup>29</sup>C. Jarzynski, "Equalities and inequalities: Irreversibility and the second law of thermodynamics at the nanoscale," Annu. Rev. Condens. Matter Phys. 2, 329 (2011).
- $^{30}\mathrm{U}$ . Seifert, "Stochastic thermodynamics, fluctuation theorems and molecular machines," Rep. Prog. Phys. 75, 126001 (2012).
- $^{\bf 31}$  C. Van den Broeck and M. Esposito, "Ensemble and trajectory thermodynamics: A brief introduction," Physica A 418, 6 (2015).
- <sup>32</sup>R. Marsland and J. England, "Limits of predictions in thermodynamic systems: A review," Rep. Prog. Phys. 81, 016601 (2017).
- 33 U. Seifert, "Stochastic thermodynamics: From principles to the cost of
- precision," Physica A **504**, 176 (2018).

  34J. M. Horowitz and T. R. Gingrich, "Thermodynamic uncertainty relations" (2019) constrain non-equilibrium fluctuations," Nat. Phys. 16, 15 (2019).
- 35 N. Shiraishi, K. Funo, and K. Saito, "Speed limit for classical stochastic processes," Phys. Rev. Lett. 121, 070601 (2018).
- <sup>36</sup>S. Ito, "Stochastic thermodynamic interpretation of information geometry," Phys. Rev. Lett. 121, 030605 (2018).
- <sup>37</sup>S. B. Nicholson, A. del Campo, and J. R. Green, "Nonequilibrium uncertainty principle from information geometry," Phys. Rev. E 98, 032106 (2018).
- <sup>38</sup>G. Falasco and M. Esposito, "Dissipation-time uncertainty relation," Phys. Rev. Lett. 125, 120604 (2020).

- 39 S. B. Nicholson, L. P. García-Pintos, A. del Campo, and J. R. Green, "Timeinformation uncertainty relations in thermodynamics," Nat. Phys. 16, 1211
- <sup>40</sup>D. A. McQuarrie, "Stochastic approach to chemical kinetics," J. Appl. Probab. 4, 413 (1967).
- <sup>41</sup>D. T. Gillespie, Markov Processes: An Introduction for Physical Scientists (Elsevier, 1991).
- <sup>42</sup>B. Munsky and M. Khammash, "The finite state projection algorithm for the solution of the chemical master equation," J. Chem. Phys. 124, 044104 (2006).
- 43 S. Peles, B. Munsky, and M. Khammash, "Reduction and solution of the chemical master equation using time scale separation and finite state projection," J. Chem. Phys. 125, 204104 (2006).
- <sup>44</sup>Z. G. Nicolaou, T. Nishikawa, S. B. Nicholson, J. R. Green, and A. E. Motter, "Non-normality and non-monotonic dynamics in complex reaction networks," Phys. Rev. Res. 2, 043059 (2020).
- 45 W. H. Press, S. A. Teukolsky, W. T. Vetterling, and B. P. Flannery, Numerical Recipes: The Art of Scientific Computing, 3rd ed. (Cambridge University Press,
- $^{\bf 46}{\rm D.~T.}$  Gillespie, "A general method for numerically simulating the stochastic time evolution of coupled chemical reactions," J. Comput. Phys. 22, 403 (1976).
- <sup>47</sup>D. T. Gillespie, "Exact stochastic simulation of coupled chemical reactions," J. Phys. Chem. 81, 2340 (1977).
- <sup>48</sup>D. T. Gillespie, "Stochastic simulation of chemical kinetics," Annu. Rev. Phys. Chem. 58, 35 (2007).
- <sup>49</sup>D. A. McQuarrie, "Kinetics of small systems. I," J. Chem. Phys. 38, 433 (1963); D. A. McQuarrie, C. J. Jachimowski, and M. E. Russell, "Kinetics of small systems. II," ibid. 40, 2914 (1964).
- <sup>50</sup>D. T. Gillespie, "A rigorous derivation of the chemical master equation," Physica A 188, 404 (1992).
- <sup>51</sup>L. O. Hedges, R. L. Jack, J. P. Garrahan, and D. Chandler, "Dynamic orderdisorder in atomistic models of structural glass formers," Science 323, 1309 (2009). <sup>52</sup>V. Lecomte, C. Appert-Rolland, and F. van Wijland, "Thermodynamic formal-
- ism for systems with Markov dynamics," J. Stat. Phys. 127, 51 (2007). 53 C. Y. Mou, J. l. Luo, and G. Nicolis, "Stochastic thermodynamics of nonequi-
- librium steady states in chemical reaction systems," J. Chem. Phys. 84, 7011
- <sup>54</sup>T. Schmiedl and U. Seifert, "Stochastic thermodynamics of chemical reaction networks," J. Chem. Phys. 126, 044101 (2007).
- <sup>55</sup>M. Polettini and M. Esposito, "Irreversible thermodynamics of open chemical networks. I. Emergent cycles and broken conservation laws," J. Chem. Phys. 141,
- $^{56}$ R. Rao and M. Esposito, "Nonequilibrium thermodynamics of chemical reaction networks: Wisdom from stochastic thermodynamics," Phys. Rev. X 6, 041064 (2016).
- <sup>57</sup>R. Rao and M. Esposito, "Conservation laws and work fluctuation relations in chemical reaction networks," J. Chem. Phys. 149, 245101 (2018).
- <sup>58</sup>C. Maes, "Local detailed balance," SciPost Phys. Lect. Notes **32**, 32 (2021).
- <sup>59</sup>L. Peliti and S. Pigolotti, *Stochastic Thermodynamics* (Princeton University Press, 2021).
- 60 J. L. Lebowitz and H. Spohn, "A Gallavotti-Cohen-type symmetry in the large deviation functional for stochastic dynamics," J. Stat. Phys. 95, 333 (1999).
- $^{\bf 61}{\rm U.}$  Seifert, "Entropy production along a stochastic trajectory and an integral fluctuation theorem," Phys. Rev. Lett. 95, 040602 (2005).
- $^{\bf 62}{\rm P.}$  Gaspard, "Time-reversed dynamical entropy and irreversibility in Markovian random processes," J. Stat. Phys. 117, 599 (2004).
- <sup>63</sup>A. Milchev, K. Binder, and D. W. Heermann, "Fluctuations and lack of selfaveraging in the kinetics of domain growth," Z. Phys. B: Condens. Matter 63, 521
- <sup>64</sup>T. Vicsek and F. Family, "Dynamic scaling for aggregation of clusters," Phys. Rev. Lett. 52, 1669 (1984); F. Family and T. Vicsek, "Scaling of the active zone in the Eden process on percolation networks and the ballistic deposition model," J. Phys. A: Math. Gen. 18, L75 (1985).
- 65 L. B. Newcomb, M. Alaghemandi, and J. R. Green, "Nonequilibrium phase coexistence and criticality near the second explosion limit of hydrogen combustion," J. Chem. Phys. 147, 034108 (2017); L. B. Newcomb, M. E. Marucci, and J. R. Green,

- "Explosion limits of hydrogen-oxygen mixtures from nonequilibrium critical points," Phys. Chem. Chem. Phys. 20, 15746 (2018).
- <sup>66</sup>A. Blokhuis, D. Lacoste, and P. Nghe, "Universal motifs and the diversity of autocatalytic systems," Proc. Natl. Acad. Sci. U. S. A. 117, 25230 (2020).
- <sup>67</sup>S. B. Nicholson, M. Alaghemandi, and J. R. Green, "Learning the mechanisms of chemical disequilibria," J. Chem. Phys. 145, 084112 (2016); "Effects of temperature and mass conservation on the typical chemical sequences of hydrogen oxidation," 148, 044102 (2018); S. B. Nicholson, R. A. Bone, and J. R. Green, "Typical stochastic paths in the transient assembly of fibrous materials," J. Phys. Chem. B 123, 4792 (2019).
- <sup>68</sup> U. Seifert, "Fluctuation theorem for birth-death or chemical master equations with time-dependent rates," J. Phys. A: Math. Gen. 37, L517 (2004).
- 69 S. Das Sarma and P. Tamborenea, "A new universality class for kinetic growth: One-dimensional molecular-beam epitaxy," Phys. Rev. Lett. 66, 325 (1991).
- <sup>70</sup> H. Qian and L. M. Bishop, "The chemical master equation approach to nonequilibrium steady-state of open biochemical systems: Linear single-molecule enzyme kinetics and nonlinear biochemical reaction networks," Int. J. Mol. Sci. 11, 3472 (2010).
- <sup>71</sup>P. Minnhagen, B. J. Kim, and H. Weber, "Evidence of two distinct dynamic critical exponents in connection with vortex physics," Phys. Rev. Lett. 87, 037002 (2001).
- <sup>72</sup>J. M. Horowitz and J. L. England, "Spontaneous fine-tuning to environment in many-species chemical reaction networks," Proc. Natl. Acad. Sci. U. S. A. **114**, 7565 (2017).